



Customized Woven Carbon Fiber Electrodes for Bioelectrochemical Systems—A Study of Structural Parameters

Liesa Pötschke¹, Philipp Huber², Georg Stegshuster³, Sascha Schriever², Norman Kroppen⁴, Joyce Schmatz⁵, Thomas Gries², Lars M. Blank¹, Peter Farber⁴ and Miriam A. Rosenbaum^{6,7*}

¹Institute of Applied Microbiology, ABBt—Aachen Biology and Biotechnology, RWTH Aachen University, Aachen, Germany, ²Institut für Textiltechnik, RWTH Aachen University, Aachen, Germany, ³Institut für Textiltechnik Augsburg gGmbH, Augsburg, Germany, ⁴Institute of Modelling and High-Performance Computing, Hochschule Niederrhein University of Applied Sciences, Krefeld, Germany, ⁵MaP—Microstructure and Pores GmbH, Aachen, Germany, ⁶Bio Pilot Plant, Leibniz Institute for Natural Products Research and Infection Biology, Hans-Knöll-Institute, Jena, Germany, ⁷Faculty of Biological Sciences, Friedrich Schiller University, Jena, Germany

OPEN ACCESS

Edited by:

Yan Li,
Florida State University, United States

Reviewed by:

Mohanakrishna Gunda,
Indian Institute of Technology Madras,
India
Sunil A. Patil,
Indian Institute of Science Education
and Research Mohali, India

*Correspondence:

Miriam A. Rosenbaum
miriam.rosenbaum@leibniz-hki.de

Specialty section:

This article was submitted to
Biochemical Engineering,
a section of the journal
Frontiers in Chemical Engineering

Received: 22 September 2021

Accepted: 19 April 2022

Published: 10 May 2022

Citation:

Pötschke L, Huber P, Stegshuster G,
Schriever S, Kroppen N, Schmatz J,
Gries T, Blank LM, Farber P and
Rosenbaum MA (2022) Customized
Woven Carbon Fiber Electrodes for
Bioelectrochemical Systems—A Study
of Structural Parameters.
Front. Chem. Eng. 4:765682.
doi: 10.3389/fceng.2022.765682

Commercial carbon fiber (CF) fabrics are popular electrode materials for bioelectrochemical systems (BES), but are usually not optimized for the specific application. This study investigates BES-relevant material characteristics on fabric level, such as weave types and weave parameters. The two contrasting weave types plain and leno weave were characterized with respect to their envisaged application types: 1) BES with mainly advective flow regimes and 2) stirred systems, which could benefit from fluid flow through a fabric electrode. Experiments with batch and continuously fed pure cultures of *Geobacter sulfurreducens* PCA and *Shewanella oneidensis* MR-1 reveal that μm -scale electrode topologies are of limited use for the thick biofilms of *G. sulfurreducens*, but can boost *S. oneidensis*' current generation especially in batch and fed-batch reactors. For advective flow regimes, deeper layers of biofilm inside microporous electrodes are often mass transport limited, even with thin biofilms of *S. oneidensis*. Therefore, low porosity plain weave electrodes for advective flow operation as in wastewater treating BES should be thin and flat. A trade-off between maximized current density and electrode material utilization exists, which is optimized exemplarily for an advective flow operation. For stirred BES of biotechnological applications, a flow-through of electrolyte is desired. For this, leno weave fabrics with pores at cm-scale are produced from 100% CF for the first time. In a preliminary evaluation, they outperform plain weave fabrics. Mass transfer investigations in stirred BES demonstrate that the large pores enable efficient electrode utilization at lower power input in terms of stirring speed.

Keywords: carbon fiber, woven electrode, porosity, *Shewanella oneidensis*, *Geobacter sulfurreducens*, bioelectrochemical system

Abbreviations: BES, bioelectrochemical system; CF, Carbon fiber; CM, multifilament roving (a type of CF); $j_{\text{max}2D}$, maximum electrical current density normalized to 2D projected surface area (two-sided electrode); $j_{\text{weight-specific}}$, electrical current normalized to electrode weight; $K_{S,\text{app}}$, apparent half-saturation constant; MFC, microbial fuel cell; PAN, polyacrylonitrile; SB, stretch-broken yarn (a type of CF).

1 INTRODUCTION

Bioelectrochemical systems (BES) utilize the metabolism of electroactive bacteria for the green generation of electricity, chemicals, and other added values such as wastewater treatment and biosensing (Santoro et al., 2017). These bacteria are able to transfer electrons to or from a solid electrically conductive surface, such as an electrode. In the most popular BES type, the microbial fuel cell (MFC), electroactive microbial biofilms generate electricity from organic matter at the bioanode (Lovley, 2006).

Commercial carbonaceous materials are by far the most common electrode materials for BES (Guo et al., 2015; Santoro et al., 2017). Among these, carbon fiber (CF) based materials are especially versatile. CF fabrics can be customized to a great extent regarding their flexibility, porosity, mechanical stability, and electrical conductivity (Adanur, 2001; Morgan, 2005; Gries et al., 2015), and by that, they offer important features for three-dimensional reactor integration of the electrode material. One CF consists of several thousands of filaments, each with a diameter of 5–7 μm (Morgan, 2005). In the most common fiber type—the continuous multifilament (CM)—the filaments are endless and parallel. Yarn thickness is reported as, e.g., 3 K (=3,000 filaments per yarn). In the less common fiber type—the stretch-broken yarn (SB)—filament

pieces of a few cm length are tightly twisted to form a yarn. The thickness usually does not exceed a 1 K equivalent.

A previous study has demonstrated the diversity of material characteristics on fiber level and elucidated possible influences on bacterial current generation in BES (Pötschke et al., 2019). For instance, the choice of the fiber type and its carbon content greatly influenced the bacteria-electrode interaction. Processing CF into textile structures generates an enormous range of electrode properties such as porosity, mechanical stability, and areal weight. Especially in slow flow regimes, macro- and microstructures of the electrode may influence chemical species transport considerably and thus, also bacterial current production. It seems likely that structural variations on fabric level may be exploited to boost BES electrode performance. The four basic weave patterns plain, twill, satin, and leno weave create a wide range of different fabric characteristics. The simplest pattern is the plain weave, a 2 yarn system, which is identical in both x- and y-direction (Adanur, 2001; Kowtsch et al., 2011). Twill and satin weave have a reduced rigidity, but higher flexibility due to less yarn crossing points. But overall, the scales of surface topography (μm -range structures) of plain, twill and satin weave are similar. The leno weave features a 3 yarn system (Kowtsch et al., 2011; Gries et al., 2015). Here, one weft and two intertwining warp yarn systems create an excellent resistance to yarn slippage, which in turn enables the

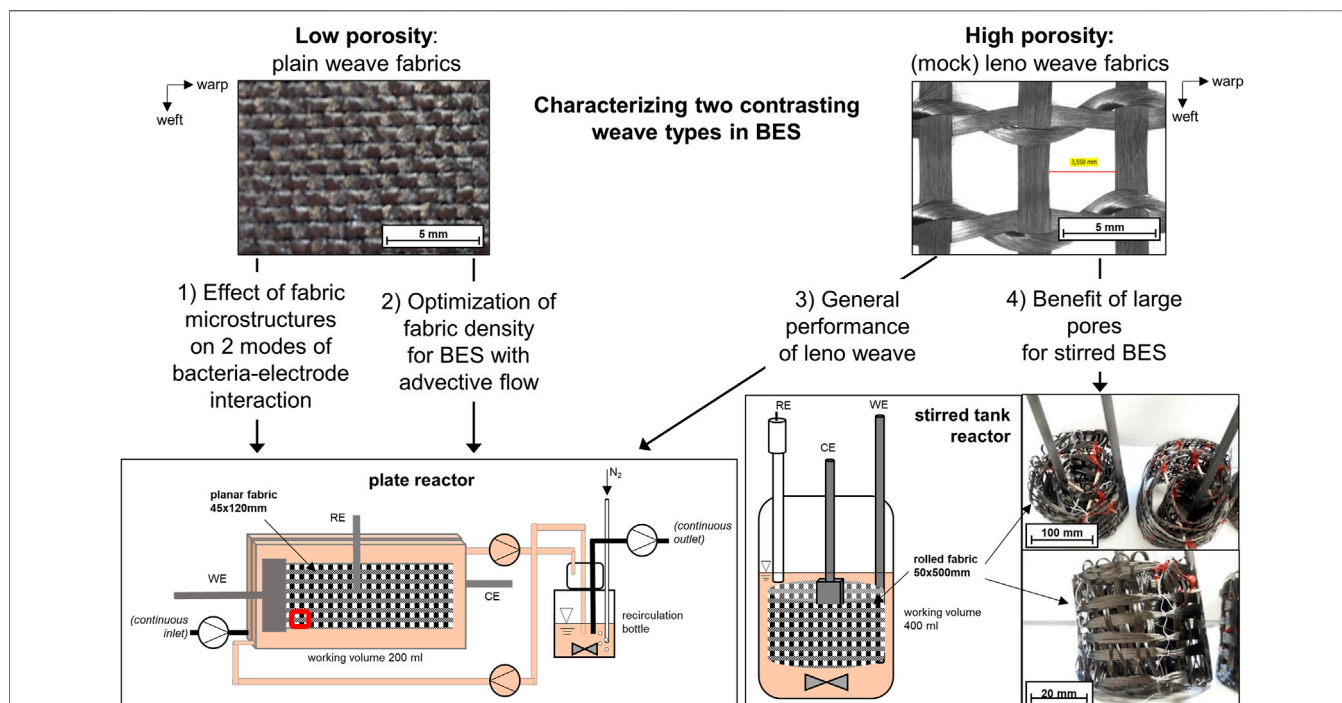


FIGURE 1 | Scope of the study and bioelectrochemical setups. The study evaluates two contrasting carbon textile electrodes: a plain weave fabric—of typically low porosity—and a leno weave fabric, which can achieve inter-yarn gaps at cm scale (top photographs). Warp and weft yarn direction are indicated. The two weave types are characterized for applications in 1) BES with mainly advective flow regimes (left, plate reactor) and 2) stirred systems (right, stirred tank reactor), which could benefit from fluid flow across the electrode. Plain fabrics are used to investigate the importance of μm topologies for two modes of electron transfer by electroactive bacteria and, the fabric density of these low-porosity fabrics is exemplarily optimized. Leno and mock leno fabrics are used to demonstrate the benefit of high porosity fabrics for stirred tank BES.

manufacturing of highly open fabrics with pore/gap sizes in the centimeter scale. The tight yarn interconnections also result in a very low electrical resistance of this fabric. Examples of a plain and a leno fabric structure are depicted in **Figure 1**.

In numerical simulation studies conducted by Farber and coworkers, both plain (Farber et al., 2021) and leno (Pötschke et al., 2018) configurations outperformed other weave types as potential electrode materials for BES. The numerical model was based on a 40 μm thick biofilm of metabolically active *G. sulfurreducens*. A summary of the most relevant results is included in the **Supplementary Material** of this manuscript (**Supplementary Table S1**). One plain and two leno fabrics achieved the highest power outputs per 2D electrode surface, which was explained by their ability to sustain the greatest biofilm surfaces with respect to this area. Leno fabrics, with their very open macroscopic holes, reached by far the highest power densities with respect to the—microscopic—fiber surface, i.e., achieved the best material usage.

With this information, we went out to further explore these two weave types of opposing, but interesting material characteristics. The scope of this study is the experimental assessment of the plain and leno fabrics' suitability for specific BES applications. Two main application types are distinguished, with 1) applications that involve particulate matter and a strong biofilm formation (e.g., in wastewaters), and 2) particulate-free electrolytes (except for suspended cells) such as in biosensors or bioelectrosynthesis with pure cultures. Here, typically the biofilm thickness on electrodes is limited to few micrometers and/or bacteria use mediator-based electron transfer to interact with electrodes.

First, the bacteria-electrode interactions with plain fabrics of two different microstructures are characterized using batch and continuously fed cultures of *Shewanella oneidensis* MR-1 and *Geobacter sulfurreducens* PCA to derive possible limitations. The two well described model organisms are representatives of the

two main electron transfer mechanisms, biofilm-based and mediated electron transfer (neglecting the typically thin, single cell layer biofilms formed by *S. oneidensis* in anaerobic systems). Next, one type of plain fabric is exemplarily optimized regarding weave density and characterized in advective flow regimes. Finally, leno fabrics are produced from 100% CF for the first time in this study. They are characterized regarding their large pores and the potential benefit that these present for stirred BES.

2 MATERIALS AND METHODS

2.1 Carbon Fiber Fabrics

All CF in this study were based on the precursor polyacrylonitrile (PAN). **Table 1** contains all technical specifications of woven CF fabrics used in this study, details of underlying fibers can be found in **Supplementary Table S3**. Two of the used CM (continuous multifilaments, Torayca[®] T300-40B and TR 30S 3L) were obtained from different suppliers, but have equivalent technical specifications. Since plain fabric electrodes that were based on either of these two CM, also showed highly similar performance, they were considered technical replicates and were combined under the sample name "plain-CM1". Two larger series of fabrics (all mock leno fabrics and all plain fabrics with varying yarn thickness/yarn input) were manufactured in-house on a Jacquard weaving machine NFJK 2 53 (Jakob Müller AG Frick, Switzerland). The leno fabric leno-CM1 was produced as half-cross leno with 4 yarns/cm in both weft and warp direction. Other fabrics were obtained from commercial suppliers as indicated. To our knowledge, full CF fabrics with leno and mock leno weave were produced in this work for the first time. All fabrics made from CM and the fabric leno-SB, were desized prior to use (pyrolysis in N₂, 500°C for 20 min or 3 h for larger fabric pieces of experiments **Section 3.4**). This process removes the

TABLE 1 | CF fabrics used in this study.

Name (weave pattern - fiber)	Cover factor ^a [%]	Inter-yarn gap [mm]		Fiber specification
		Warp	Weft	
Plain-SB1	94	0.12 ± 0.03	0.17 ± 0.05	Carbonized at fabric level. Fabric specifications: Zoltek™ PX30 PW06 Zoltek Corporation, MO, United States
Plain-CM1	83	0.42 ± 0.06	0.39 ± 0.05	Torayca [®] T300-40B, Toray Industries Inc., Japan (3K CM) or ^b TR 30 S 3L, Mitsubishi Chemical Carbon Fiber and Composites, Inc., Japan/United States (3K CM)
Plain-CM2 (various weave parameters)	<i>Fabric densities were calculated instead of porosity (details see results 3.2)</i>			
Leno-CM1	55	3.43 ± 0.17	3.97 ± 0.18	Torayca [®] T300-40B, Toray Industries Inc., Japan (3K CM)
Leno-SB2	n.a.	n.a.	n.a.	Zoltek™ PX35YZ0106 Zoltek Corporation, MO, United States
Mock-CM2 (various weave parameters ^c)	61–90	3.4–8.7	3.4–5.8	Tenax [®] HTA40 E13, Toho Tenax Europe, Germany (3, 6, or 12K CM)

Sample denominations contain weave pattern (plain, leno, or mock leno) and the underlying fiber (SB, stretch-broken yarn; CM, continuous multifilaments).

^aCover factor is a measure of porosity for fabrics (areal ratio of surface covered by yarns to the total fabric surface, i.e., a high cover factor translates to a low porosity). Numbers as in CM1, CM2, refer to CM with different technical specifications. Details on the underlying CM are given (3K = 3,000 filaments per roving), more technical information can be found in **Supplementary Table S3**. All Plain-CM2 and all Mock-CM2 fabrics were produced in-house. Leno-CM1 (150 g/m², half-cross leno with 4 yarns/cm in both weft and warp direction) was produced by Güth & Wolf GmbH, Gütersloh, Germany; Leno-SB (130 g/m², half-cross leno with 4 yarns/cm in both weft and warp direction) was manually produced at ITA gGmbH, Augsburg, Germany; Plain-CM1 fabrics (200 g/m²) were produced by CARBO-TEX GmbH, Nordendorf, Germany.

^b(two equivalent CM from different manufacturers were used); ZOLTEK™ PX30 PW06 (237 g/m²) is a graphitized fabric (carbon content 99%) and was purchased from ZOLTEK Zrt., Hungary.

^cThe presented data reflect the range of porosity and inter-yarn gaps covered by all mock-CM2 fabrics; details for the single fabric samples are given in **Supplementary Table S6**.

protective polymer coating (sizing), which would interfere with bacterial current generation (Pötschke et al., 2019). Commercial SB fabrics used in this study were based on oxidized PAN (PANOX), which means they lose their sizing during the production process (Morgan, 2005). Therefore, these fabrics were not pretreated other than standard sterilization by autoclaving. Autoclaving also pre-wetted the fabrics, which reduced the formation of an air film upon immersion in the electrolyte. Fabric porosity is defined by the cover factor (areal ratio of surface covered by yarns to the total fabric surface, i.e., a high cover factor translates to a low porosity). Cover factors as well as inter-yarn gaps in weft and warp direction were determined semi-automatically from light microscopic images and photographs.

All CF electrode names contain weave pattern and the underlying CF type, e.g., “leno-SB”.

2.2 Electroactive Bacteria and Culturing Conditions

For *Shewanella oneidensis* MR-1 (ATCC[®] 700550[™]) experiments, general procedures were identical to (Pötschke et al., 2019). In brief, 1 ml of an overnight grown culture was inoculated into the reactor, which contained a modified M4 medium (Supplementary Table S4) with 18 mM lactate as sole carbon source. Precultures of *Geobacter sulfurreducens* PCA (DSMZ 12127) were grown for 3–5 days in serum bottles with 15 mM sodium acetate as carbon source and electron donor and 40 mM sodium fumarate as electron acceptor. The anaerobic (nitrogen degassed) phosphate buffered medium is provided in Supplementary Table S5 [adapted from Kim et al. (2005)]. The medium was identical for BES experiments, except for fumarate being omitted.

2.3 Bioelectrochemical Setups

All solid, compressed graphite materials like rods were purchased from Novotec GmbH, Germany, and were of grade EDM 3 (specific electrical resistivity 1.56 mΩ cm).

Two different types of BES setups were used to characterize the different CF fabrics (Figure 1).

The bioelectrochemical setup for 2D fabric electrode testing were flat-plate type reactors as described before (Pötschke et al., 2019). In brief, two rectangular frames (10 mm × 148 mm × 55 mm) contained each of the electrodes and an in-house prepared Ag/AgCl_(sat.KCl) reference electrode (0.197 V vs. SHE) and were combined to one chamber with a net liquid volume of 120 ml. A CF fabric (45 mm × 120 mm, total surface area 108 cm²) was used as working electrode and a graphite rod as counter electrode. The total electrolyte volume of 200 ml (400 ml for experiments in Sections 3.2 and 3.3) was recirculated at 20 ml/min between the plate reactor and a stirred recirculation bottle in order to allow for continuous nitrogen sparging and mixing (Figure 1). Substrates were repeatedly added in fed-batch mode whenever the current generation started to cease, until the current density did not increase any further (maximum current density j_{max}).

The plate reactor setup was furthermore used for continuous operation experiments. For this purpose, an additional inlet port was installed and the outlet was located in the recirculation bottle as schemed in Figure 1. Reactors were operated in fed-batch mode for 5–10 days to develop bacterial current generation and growth. Then, continuous feed with the respective BES medium for each organism was started and hydraulic retention times (HRT) were kept at approx. 10 h. For *G. sulfurreducens*, the complete experimental setup including feed bottles was setup inside an anaerobic chamber (Coy laboratory products, MI, United States) and all media were degassed and reducing agent was added. For *S. oneidensis*, the reactor as shown in Figure 1 was continuously sparged with N₂, but the feed was not additionally sparged. The small amount of dissolved oxygen was found to have a neglectable influence on the experiments. Feed concentrations were varied between 0.5–15 mM lactate (*S. oneidensis*) and 0.5–20 mM acetate (*G. sulfurreducens*), starting from the highest concentration and stepwise decreasing down to the lowest. Each feed concentration was maintained constant for at least 3 HRT before sampling feed bottle and reactor for offline analyses. Monod-type data fits were carried out using the software OriginPro (OriginLab Corporation, MA, United States) and the equation

$$j = \frac{j_{max} \cdot [S]}{K_{S,app} + [S]}$$

with j , current density; j_{max} , theoretical maximum current density; $[S]$, substrate concentration (equals electron donor in these experiments); $K_{S,app}$, apparent half-saturation constant, i.e., the substrate concentration at the sampling point in the reactor at half-maximum current density. When more than one independent reactor was operated, the combined dataset of all replicates was used for one non-linear fit (see Supplementary Figure S1 for fitted datasets).

Electrical current generation was strongly influenced by the ambient temperature (Supplementary Figure S2). Although the laboratory was temperature-controlled at 22.5°C, daily fluctuations of ±5°C were recorded. Therefore, current data of approx. 24 h of each steady state were averaged.

A different single-chamber setup was used for the evaluation of 3D mock leno fabrics (Figure 1). The counter electrode was a graphite plate (73 mm × 22 mm × 9 mm, total surface area 49 cm²), attached to a graphite rod and wrapped in a cation exchange membrane (CMI-7000S, Membranes International Inc., NJ, United States) to avoid short circuits. The working electrode, a CF fabric (50 mm × 500 mm, total surface area 500 cm²), was rolled around the counter electrode with the goal to evenly distribute the CF material in the electrolyte space (packing density 125 m²/m³ considering both sides of the planar fabric). The fabric pores were stabilized by either applying dots of high-temperature resistant silicone (stable up to 300°C, OBI GmbH & Co. Deutschland KG, Germany) or CF were tied at crossing points by a cotton yarn. The 3D draped structure including spaces between CF layers was stabilized by toothpicks (Figure 1). Both electrodes were attached to graphite rods (Ø 5 mm) using conductive carbon cement (Leit-C, Science Services

GmbH, Germany). Owing to the size of the CF fabric, four rods were attached in total and interconnected to avoid large potential drops within the electrode. A working volume of 0.4 L was used, just enough to cover the electrodes and allow stirring at the reactor bottom [3 cm magnetic stirrer (Carl Roth, Germany) at 100 or 520 rpm as indicated]. Furthermore, a Ag/AgCl_(sat. KCl) reference electrode and a sparger for continuous N₂ supply were located near the reactor wall. Control experiments were run with 1) a plain-SB fabric, configured as fabric roll as well and 2) a non-porous graphite comb as working electrode [e.g., as in Schmitz et al. (2015)].

For all experiments, Chronoamperometry (CA) was performed with a poised potential of +0.2 V vs. Ag/AgCl_(sat. KCl) (potentiostats: VMP-3, BioLogic Science Instruments, France; Ivium-n-Stat, Ivium Technologies, Netherlands). The CA was interrupted by cyclic voltammetry measurements (CV; 2 mV/s from +0.5 V to -0.5 V vs. Ag/AgCl_(sat. KCl), three cycles) every 72 h, which are visible as peaks in some CA graphs. CV data were collected as control only and will not be reported here. Current and power densities are normalized to the 2D surface area throughout this study (both sides of a planar electrode equivalent or the complete accessible surface area of a compact graphite comb/rod).

Offline analyses. Regularly, the optical density at 600 nm (OD₆₀₀), organic acids via HPLC (Metab-AAC column, 300 mm × 7.8 mm, Isera GmbH, Germany; in 5 mM H₂SO₄ mobile phase, 0.6 ml/min, 30°C), and pH were monitored during the experiments as control. Ambient temperature was monitored in a reference bottle with 200 ml H₂O using a Pt100 resistance thermometer. For cross-section imaging of selected samples, electrode pieces of approx. 1 cm × 2 cm were delimited by adding silicone traces prior to the experiment (location depicted in **Figure 1**). The pieces were cut out after the experiment, washed with deionized water to remove planktonic cells and immediately stored in liquid nitrogen. Cross-sections of the samples were prepared, basically following the protocol described in Schmatz et al. (2017). Different to Schmatz et al. (2017), the Cryo-BIB milled sample cross-sections were not sputter coated allowing for controlled sublimation during the SEM investigation. Microbial cell bodies were made visible by carefully raising the temperature for a short time, which led to sublimation of surrounding water. Membranes of non-fixed cells were not stable and left negative hollow imprints or only the extracellular biofilm matrix was visible, but chemically fixed cells (glutaraldehyde 2.5%, 4°C overnight, OsO₄ 1%, 4°C, 2 h, both in 1 M sodium phosphate buffer) emerged intact from the sublimating water.

3 RESULTS

3.1 Influence of Microstructures in Plain Weave Electrodes on Modes of Bacterial Electron Transfer

First, we evaluated the influence of structural differences of CF electrodes based on the two fundamentally different CF types on

the performances of the two model organisms *G. sulfurreducens* PCA and *S. oneidensis* MR-1 in BES. Plain fabrics of similar areal weight were selected. A stretch-broken yarn (SB) based fabric is compared against a CM based fabric.

Apart from fed-batch plate reactors, we also operated continuous feed experiments to deduct the key kinetic parameters for the electroactivity of the two bacterial biocatalysts. HRT were kept constant and substrate concentrations in the feed bottle were varied. Plots of current density vs. electron donor concentration in the reactor exhibited Monod-type behavior of substrate-limited systems as described elsewhere (Torres et al., 2007; Torres et al., 2010).

With *Geobacter*, differences between j_{\max} of the two CF electrodes are small (**Table 2**). Furthermore, j_{\max} of CF electrodes is hardly higher than j_{\max} achieved with planar graphite. Besides the small differences, the plain-SB fabric was defined as the best performing material. However, j_{\max} for *G. sulfurreducens* calculated from continuous operation seem to underestimate real achievable current densities, since higher values are reached in batch operation. In fact, current generation became unstable in most reactors when high acetate concentrations were fed and high current values were challenging to record at all for continuous operation.

j_{\max} with *S. oneidensis* is roughly one order of magnitude lower than with *G. sulfurreducens* for all electrodes (0.1–0.8 vs. 3.9–4.7 A/m² in batch mode, respectively, **Table 2**), which has been observed elsewhere (Engel et al., 2019). Differences between structurally different electrodes made from SB and CM are more pronounced for this organism. With plain-SB electrodes, current generation reaches similar levels in batch and continuously fed reactors. With plain-CM1 electrodes, however, current generation is clearly enhanced in continuous operation, reaching similar performance as plain-SB electrodes. Furthermore, the different CF electrodes achieve 2–3-fold higher j_{\max} than planar graphite electrodes in other setups.

Apparent half-saturation constants $K_{S,app}$ with *G. sulfurreducens* cultures are comparable between different CF materials considering the statistical errors (**Table 2**). In *S. oneidensis* cultures, again, structural electrode difference are reflected in the kinetic data: plain-SB fabrics yield a reduced $K_{S,app}$ compared to plain-CM1 fabrics.

3.2 Bacterial Exploitation of Microscopic Three-Dimensional Surface Area Inside Plain Weave Electrodes

Next, we explored the actual usability of the structural electrode surface for bacterial interaction. Flow-through of an electrolyte through a porous electrode yields improved electrode performances, because chemical species transport is improved. However, this flow regime is not applicable or feasible for many BES architectures, since it increases the design complexity. In addition, biofilm-based systems employ comparatively thick biofilms and particulate matter (as in wastewater), which may clog electrode pores. Out of the commercially available weave patterns, the plain weave is a straightforward option for applications, however, it only allows for advective flow. It is

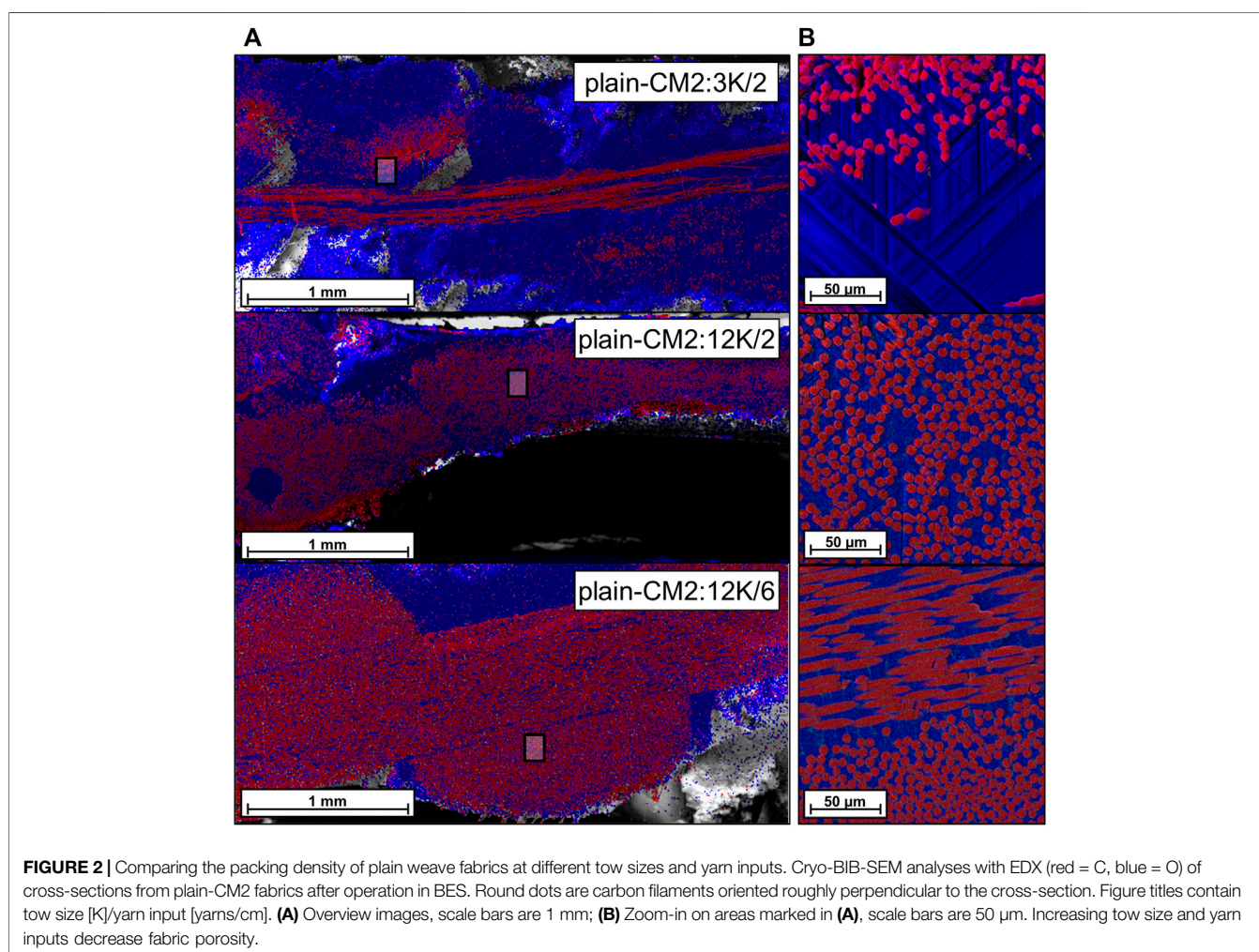
TABLE 2 | Maximum current densities j_{\max} [A/m^2] and apparent half-saturation constants $K_{S,app}$ [mM] for *G. sulfurreducens* and *S. oneidensis* in batch and continuously operated plate reactors with woven CF electrodes.

Parameter	Plain-SB		Plain-CM1		Graphite	
	Batch	Continuous	Batch	Continuous	Batch	Continuous
GS						
j_{\max}	4.7 ± 0.9	4.4 ± 0.3	4.2/4.4	3.2 ± 0.2	3.9 ± 0.9 Engel et al. (2019)	3.1 Nevin et al. (2008) ^a
$K_{S,app}$	—	1.87 ± 0.28	—	1.61 ± 0.39	—	n.a.
n	5	4	2	2	3	2
SO						
j_{\max}	0.8 ± 0.2	0.7 ± 0.1	0.5 ± 0.2	0.9 ± 0.04	$0.1 / 0.3^b$ [0.3 ± 0.1 Engel et al. (2019)]	n.a.
$K_{S,app}$	—	0.26 ± 0.08	—	0.53 ± 0.11	—	n.a.
n	4	2	4	4	2 (3)	n.a.

Values from batch operation are arithmetic means and the deviation of mean from the given number of replicates (n). Values for continuous operation were obtained from Michaelis-Menten fit to the combined dataset of all replicates and include errors from this fit calculation. Fitted datasets can be found in **Supplementary Figure S1**. $K_{S,app}$ refers to substrates acetate in *G. sulfurreducens* (GS) and lactate in *S. oneidensis* (SO) experiments. Woven fabrics are plain weave fabrics, based on either SB, stretch-broken yarn, or CM, continuous multifilament. All electrodes were poised at 0.2 V vs. Ag/AgCl except for:

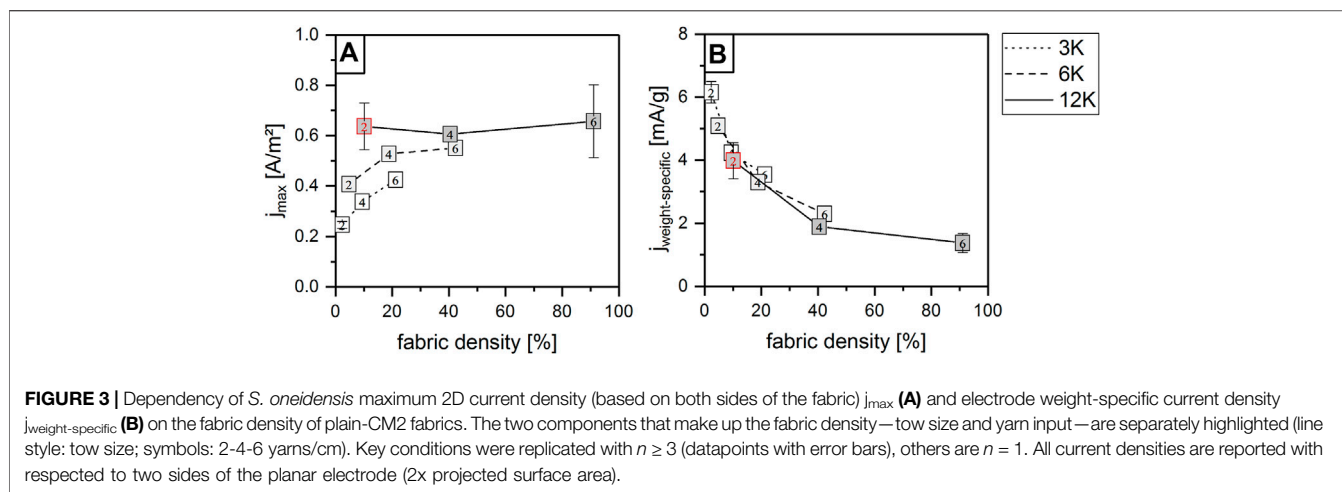
^aMFC mode with ferricyanide cathode.

^bSingle chamber BES with graphite comb as working electrode (this work). All current densities are reported with respect to two sides of the planar electrode (2x projected surface area).



the simplest weave pattern and causes a comparably low pressure drop in this flow regime (**Supplementary Table S2**). To evaluate the range of performance of this weave type in detail, a systematic screening of plain-CM2 fabrics with differing weave parameters

was conducted. The two parameters that were varied were yarn thickness (3, 6, or 12 K) and yarn input (2, 4, or 6 yarns/cm, applied simultaneously for both warp and weft yarn density). This yielded different fabric densities that covered a typical range of



electrode porosity and thickness as used in BES. The fabric densities describe the coverage of the 2D projected surface area by CF material in percent [%] [calculation after Walz and Luibrand as in Kowtsch et al. (2011)]. Therefore, a low yarn input with low yarn thickness (configuration 3 K/2) achieves the highest porosity (Figure 2, top). However, CM yarns fall flat in a woven fabric, therefore a good areal coverage was still achieved with low yarn input when the thickest (12 K) yarns were used (Figure 2 middle). Increasing the yarn input with 12 K yarns only increased the packing density of filaments both along the electrode cross section (space between single filaments, compare Figure 2 bottom) and with respect to the projected surface area of the electrode (number of filaments per electrode surface).

The fabrics were evaluated in the plate reactor set-up with *S. oneidensis* as the test organism. J_{\max} is increasing with fabric density, but reaches a plateau for thick yarns and high fabric densities (Figure 3). In other words, the highest j_{\max} is reached with a complete areal coverage of CF material, and is then almost independent from filament packing density. Thus, the increase in inner three-dimensional surface area from 12 K/2 to 12 K/6 configuration is barely exploited by *S. oneidensis*. The weight-specific current (usage of available electrode material) is rapidly decreasing with fabric density. The optimum is at the lowest areal coverage, i.e., is achieved with the material plain-CM2:3K/2 with the highest porosity. The best trade-off between high j_{\max} and material usability is the configuration 12 K yarn at 2 yarns/cm, i.e., the thickest yarn with low yarn input (Figure 3, marked red).

Selected samples of the configuration shown in Figure 3 (the two most extremes and the considered optimum) were further treated to investigate the presence of bacterial cells between the filaments. Bacterial cells or their imprints (for explanation see Section 2.3) were detected in all cross sections. The images shown in Figure 4 were taken from the center of the fabric cross sections, i.e., show the innermost filaments of the samples. Bacterial cells seemed to be present even inside the tightest packed material plain-CM2:12K/6 (Figure 4, right).

3.3 Preliminary Evaluation of Porous Leno Fabrics in Advective Flow Regimes

In recent years, more BES applications with particulate-free electrolytes (except for suspended cells) and mediator-based electron transfer have emerged, especially for biotechnological applications with microbial pure cultures. These applications may benefit from more porous electrodes and an actual flow-through of the electrolyte. Installing macroscopic pores in standard plain weave fabrics greatly impacts fabric stability and seems not feasible. In contrast, leno fabrics intrinsically feature exceptionally large pores (as inter-yarn gaps) in the cm scale. Additionally, they feature a good stability, i.e., resistance to shear deformation and yarn slippage, resulting from two warp yarns being twisted around each other at every crossing point (Figure 1). A positive side-effect of the tight yarn interconnections is a low electrical resistance of the fabric compared to, e.g., a plain fabric with similarly large pores. In a preliminary experiment in stirred batch reactors with *S. oneidensis*, j_{weight} was strongly impeded when half of the yarns of a plain fabric (200 g/m^2) were removed, whereas a leno fabric (150 g/m^2) made from identical CF exceeded j_{weight} of the original plain fabric (Pötschke et al., 2018).

At present, however, leno fabrics are not commercially available as full CF fabrics. Therefore, the used fabrics were custom provided in small quantities within a publicly funded project by GÜth & Wolf GmbH (leno-CM1) and ITA Augsburg gGmbH (leno-SB). To evaluate the effect of macroscopic porosity, we also used mock leno fabrics, which mimic the high porosity of the leno fabrics, but have a standard 2-yarn system and can therefore be produced more readily on standard weaving looms. Our in-house produced mock leno fabrics (mock-CM2) reach porosities close to the values of the leno-CM1 fabric and have comparable inter-yarn gaps (Table 1). They miss, however, the tight yarn connection at crossing points, which strongly impedes the conductive properties of the mock leno compared to the true leno fabric. Owing to limited sample amounts, only single experiments of true leno fabrics were performed in the plate reactor setup in order to assess their performance (Figure 5). Leno-CM1 achieved 0.4 A/m^2 and 5.5 mA/g , leno-SB achieved 0.6 A/m^2 and 9 mA/g . Both leno fabrics achieved higher current

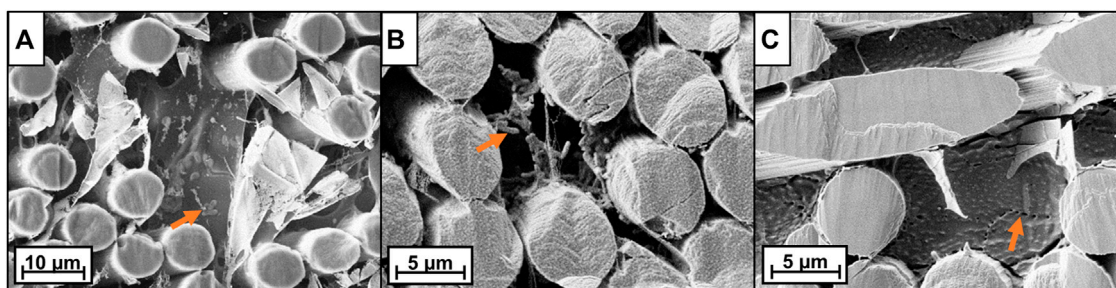


FIGURE 4 | Sublimated Cryo-BIB-SEM images of CF fabric cross-section with *S. oneidensis* biofilms grown in BES. Samples are plain-CM2:12K/2 [(A) non-fixed cells; (B) fixed cells, sputtered with tungsten] and plain-CM2:12k/6 [(C), non-fixed cells]. Fixed cells are visible between carbon filaments and indicated in (B). Membranes of non-fixed cells were not stable and mainly left negative hollow imprints [indicated in (C)] or only the extracellular biofilm matrix was visible [indicated in (A)]. Scale bars are 4 μm (A) and 2 μm (B,C).

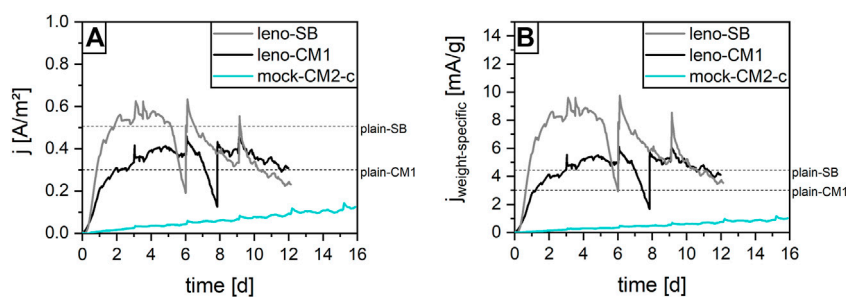


FIGURE 5 | Performance of leno fabrics and mock leno fabrics in plate reactors with *S. oneidensis* (fed-batch). Current is normalized to 2D projected electrode area (both sides of the fabric) (A) and electrode weight (B). Sharp current drops and increases are results from electron donor depletion and new addition. All sample names include the fiber type (CM or SB). Dotted lines represent the j_{max} reference performance of plain weave fabrics made from equivalent fibers as the two leno fabrics. Leno-CM1 and leno-SB were single experiments; mock-CM2-c is a representative graph from $n = 3$.

densities than plain fabrics made from equivalent (plain-CM1) or similar (plain-SB) yarns (dotted lines). Their advantage over plain fabrics was even higher comparing j_{weight} . Mock-CM2, although having similar inter-yarn gaps as leno-CM1, generated considerably lower current densities in the given experiment duration, but showed a steadily increasing current generation. With a high probability, this is related to the poor electrical contact between filaments and yarns – in contrast to the leno fabric, which features tight yarn crossing points (compare **Supplementary Figure S3** and **Figure 1**).

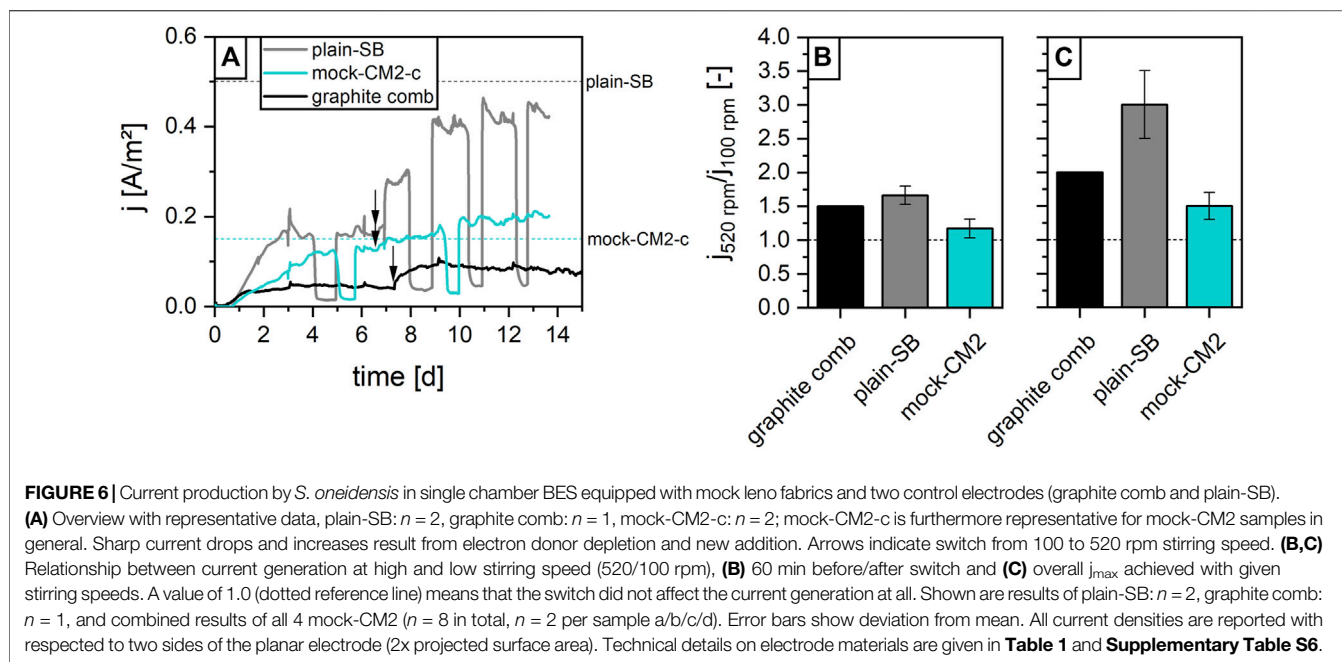
Mock-CM2, however, were able to mimic the good cross-flow dynamics of leno-CM1. This was tested in terms of the speed at which a dye would cross through the fabrics (**Supplementary Figure S5**). Mock leno fabrics were thus considered as model electrodes for the evaluation of flow through operations of porous CF electrodes, owed to their better accessibility compared to true leno fabrics.

3.4 Evaluation of Highly Porous Electrodes in Flow-Through Regimes

For biotechnological applications of electrosynthesis, BES might not be operated in advective flow systems, but rather in more traditional stirred tank reactors. Especially, here, the flow through properties of an electrode material will greatly impact fluid

dynamics and BES performance. Therefore, highly porous mock-CM2 fabrics (details see **Table 1**; **Supplementary Table S6**) were installed in stirred BES and evaluated with *S. oneidensis*. Control fabrics included a plain-SB with one order of magnitude lower porosity as well as a non-porous graphite comb. The absolute achieved current densities of mock-CM2 were lower than for the plain-SB control (**Figure 6A**), but cannot be compared, owed to the poor electrical contact between yarns of the mock leno weave compared to plain weave as stated above. This is in accordance with the preliminary experiments in plate reactors (**Figure 5**). Therefore, in the following experiments, only the benefit of high porosity and large pores are investigated as independent material characteristics.

To evaluate the impact of the electrode porosity on fluid dynamics and overall electrode performance, the setup was first stirred at low speed (100 rpm) and switched to high speed (520 rpm) after 6.5 or 7 days. Mock-CM2 performance turned out rather independent from increased fluid mixing (**Figure 6A**). Repeated experiments with mock-CM2 samples of varying weave parameters gave similar results and were therefore combined to reflect the performance range of all mock-CM2 fabrics (**Figures 6B,C**). In contrast, the less porous controls showed a stronger increase in current generation in prompt response to increased mixing (**Figures 6A,B**). Furthermore, the controls had reached a



plateau at the lower mixing rate and were clearly boosted by the increased liquid turnover, i.e., increased their current density drastically in the long-term (**Figures 6A,C**). For the plain-SB, this resulted in a current density increase by up to 250%. This indicated that the current generation with plain fabrics, but not the mock leno fabrics, was strongly diffusion-dependent under low-speed stirring conditions limiting bacterial activity.

4 DISCUSSION

4.1 Carbon Fiber Microstructures Are Mainly Relevant for Current Generation With Thin Biofilms

The two electroactive model organisms *S. oneidensis* and *G. sulfurreducens* represent two fundamentally different ways of interaction with a solid electron acceptor. Their physiology greatly influences the charge transfer rate onto the final electron acceptor. Hence, they are representatives for the two dominating modes of electron transfer that might be utilized in BES: direct electron transfer dominated by a microbial biofilm and mediated electron transfer driven by a suspended, planktonic microbial population.

When both organisms were offered different electrode microstructures (**Section 3.1**), current generation was barely influenced in *G. sulfurreducens* cultures, but strongly in *S. oneidensis* cultures. Our findings are supported by literature data, which show varying current density on structurally slightly different electrodes with *S. oneidensis* (Kipf et al., 2013; Kipf et al., 2014), but not with *G. sulfurreducens* (Kipf et al., 2014). With *G. sulfurreducens*, in contrast, even plain graphite achieves similar j_{\max} as CF fabrics (**Table 2**). One

reason is certainly that *G. sulfurreducens* simply overgrows structures that are smaller than its biofilm thickness (Moß et al., 2019). Accordingly, simulations with a 40 μm thick *G. sulfurreducens* biofilm by (Farber et al., 2021) confirmed a direct link between total biofilm surface and power output. The simulations predicted that considerable structural alterations of CF fabric electrodes are required to increase the biofilm surface beyond the equivalent of a non-porous flat plate [i.e., $>1 \text{ m}^2/\text{m}^2$ (biofilm/2D electrode surface)]. Consequently, only stretch-broken yarns (SB) or the leno weave pattern result in high power outputs (see column 6 of **Supplementary Table S1**). In SB, the beneficial structural feature is believed to be the close to round yarn shape of SB (Farber et al., 2021)—in contrast, CM fall flat in a woven fabric. Furthermore, a beneficial combination of a high CF conductivity and the stretch-broken yarn structure has been elucidated previously as beneficial functional feature of SB (Pötschke et al., 2019). The results for *G. sulfurreducens* are consistent in batch and continuously fed cultures. Based on our observations, current generation relying on thick ($>40 \mu\text{m}$) biofilms is not expected to be greatly enhanced by microstructures and the μm scale pores as present in most commonly used CF textile electrodes. These findings fit observations of others (Jourdin and Burdyny, 2021). Such systems may, however, still benefit from, e.g., a chemically functionalized CF surface (Guo et al., 2013; Guo et al., 2014; Liu et al., 2014) or the drapeability of flexible CF materials to form three-dimensional electrodes.

S. oneidensis, in contrast, makes good use of both the functional and structural differences between CF fabrics and planar graphite, which is expressed in 2 to 3-fold higher current generation on CF fabrics (**Table 2**). The reason is probably that the thin biofilms of this organism do not cover all pores of the CF electrodes, and truly exploit the

microtopologies to form large biofilm surfaces. The direct link between biofilm and current generation described for *S. oneidensis* (Erben et al., 2021b) confirms these considerations. Interestingly, the above discussed benefits of SB fabrics apply for *S. oneidensis* cultures operated in batch mode only, whereas in continuously fed cultures, CM fabrics catch up with the performance of SB fabrics. On the other hand, $K_{S,app}$ is lower with SB fabrics, indicating a higher efficiency of current generation at low substrate concentrations. These observations are new and expand the knowledge on SB fabrics that we had generated previously (Pötschke et al., 2019). Several reasons could provoke that SB fabrics lose their benefit over CM fabrics in continuously fed cultures: Free filament ends of SB yarns enable a fast electron discharge (Pötschke et al., 2019). If the dominant mechanism hereby is mediated electron transfer, the benefit is lost due to mediator wash-out in continuously fed cultures. Furthermore, a robust electron conduction along intact monofilaments of CM might be of increasing importance in the long-term. Fully grown biofilms of *S. oneidensis* might further bridge single filaments by nanowires, similar to the function of free filament ends in SB fabrics. To reveal the exact mechanisms further experiments are required. In summary, current generation by *S. oneidensis* reacts sensitively to small electrode microstructures due to its low biofilm thickness and focus on mediated electron transfer. Tailored CF woven electrodes therefore show potential for mediator-based BES. A further functionalization of CF, such as to SB yarns, is especially beneficial for batch and fed-batch operated BES.

4.2 The Internal Space of Microporous Carbon Fiber Electrodes Is Rarely Exploited

Any porous CF-based electrode will eventually face mass transport limitations of inner biofilm layers with increasing biofilm thickness. On the way towards economically viable BES, however, this limitation needs to be minimized to achieve required productivity levels (Jourdin and Burdyny, 2021).

Here, weave parameters of plain fabrics were experimentally optimized for a good material exploitation in advective flow regimes (Section 3.2). The results reveal a quick saturation of j_{max} with increasing fabric density (Figure 3) in advective flow regimes. A high material exploitation, expressed here as current density per electrode weight $j_{weight-specific}$, is only possible with thin yarns and low yarn input, e.g., the configuration 3 K/2. Nevertheless, bacterial cell bodies were present all over the cross-section of fabrics (Figure 4), even the ones of high fabric density (e.g., plain-CM2:12K/6). All filaments, including the innermost, were thus physically accessible to *S. oneidensis*; but the inner cell layers were not contributing to current generation anymore towards the end of the experiment. The cells obviously face major substrate diffusion limitations once the outer biofilm is fully grown. Numerical simulations of substrate concentrations along a yarn cross-section support these considerations (Supplementary Figure S4). Furthermore, local acidification may contribute to the inactivity of inner biofilm layers (Erben et al., 2021a). These results are stunning, because *S. oneidensis*' biofilms usually do not exceed thicknesses of a few layers of cells.

Even with these thin biofilms, a full exploitation of the electrode volume is not achievable.

For advective flow regimes, the best trade-off between maximizing j_{max} and minimizing material input is a flat electrode with full areal coverage—similar to what has been anticipated for thicker *G. sulfurreducens* biofilms above. This goal is achieved best with a preferably larger tow size (12 K in our case, although this is still a small tow per technical definition), and a low yarn input. Fortunately, the production cost structure for CF favors this strategy: The thicker the tow, the cheaper the production and final product price (Das et al., 2016).

All things considered, a full electrode coverage, of course, can also be achieved more economically by graphite plates or equivalent structures. However, CF based electrodes are a flexible material, which may be configured into 3D shapes for use in stirred or tubular reactors (You et al., 2007; Zhuang et al., 2012; Rosa et al., 2019). Furthermore, offcut CF material from industrial processes is reusable (Stegschuster and Schlichter, 2018; Manis et al., 2021) and contributes to the drop of CF market prices (Das et al., 2016), which might further improve the economic benefit of CF application.

4.3 Macroporous Carbon Fiber Electrodes Enable a Good Electrode Material Exploitation in Stirred BES

For pure cultures or defined mixed culture applications such as microbial electrocatalysis, reactor architectures often call for flow-through of a porous electrode, e.g., in stirred reactors. In this flow regime, mass transport limitations can be overcome by a suitable combination of porous electrode architecture and fluid dynamics. This work introduces full CF leno fabrics with pores in the cm-scale for the first time and demonstrates their potential for BES with flow-through regimes. Highly porous leno outperformed plain fabrics of equivalent CF both in terms of j_{max} and material exploitation in a preliminary characterization (Figure 5). This confirms the model predictions by Farber et al. (2021) (Supplementary Table S1). An experimental series with mock leno fabrics, representing the large pores of leno fabrics, confirmed the benefit of these pores for bacteria-electrode interactions. The macroporous electrode structures are suitable for example for application in stirred tank BES reactors, since they allow for an excellent flow-through of the liquid (Figure 6) and improved mass transfer. By that, leno fabric electrodes produce a low pressure drop (Supplementary Table S2), which means, they can be operated at low power input in terms of stirring speed, and their surface is still fully available for bacterial interactions. In contrast, less porous materials that are well suited for advective flow (e.g., plain-SB), require a high stirring speed to enable a proper material exploitation. Efforts to introduce BES infrastructures into standard bioreactors are already pursued, e.g., by (Rosa et al., 2019). Therefore, further tailoring true leno fabrics for applications in BES may be promising. The production of such fabrics on commercial weaving looms has been proven feasible. Upcoming tasks to establish them for BES applications will be a functional reactor integration considering optimized fluid dynamics, as well as a

close collaboration with CF fabric manufacturers in order to establish the commercial availability of these specialty fabrics.

5 CONCLUSION

Carbon fiber woven fabrics are widely used as electrodes in BES. This work demonstrates that customizing them on fabric level is one way to drastically improve the performances of specific BES. We considered 1) BES, which feature thick biofilm communities on electrodes, therefore prevailing advective flow regimes (such as wastewater treating BES) and 2) BES using mineral media and pure cultures, featuring mainly mediated electron transfer, that may allow flow-through flow regimes with a porous electrode. For type 1, a microstructured electrode is of limited use and a closed, flat fabric structure of low volume is preferred. For type 2, electrode microstructures such as stretch-broken yarns can boost bacterial current generation. Furthermore, this study introduces highly porous leno weave fabrics, which were produced from 100% carbon fibers for the first time. These fabrics feature pores in the cm scale and are considered especially suitable as flow-through electrodes in stirred BES for diverse biotechnological applications.

DATA AVAILABILITY STATEMENT

The original contributions presented in the study are included in the article/**Supplementary Material**, further inquiries can be directed to the corresponding author.

AUTHOR CONTRIBUTIONS

The manuscript was written through contributions of all authors. LP performed all biological and comparable experiments with the CF fabrics, analyzed data and prepared the first draft of the manuscript, PH synthesized and physically characterized mock leno fabrics and edited the manuscript, GS synthesized and characterized the leno-SB fabric, analyzed data and edited the manuscript, SS desized all monofilament fabrics, discussed data and edited the manuscript, NK and PF performed the fabric performance simulations, discussed data and edited the manuscript, JS performed Cryo-BIB-SEM analysis of the fabrics, discussed data, and edited the manuscript, TG edited

REFERENCES

- Adanur, S. (2001). *Handbook of Weaving*. Boca Raton, FL, USA: CRC Press, Taylor & Francis Group.
- Das, S., Warren, J. A., West, D., and Schexnayder, S. M. (2016). Global Carbon Fiber Composites Supply Chain Competitiveness Analysis. ORNL/SR-2016/100 | NREL/TP-6A50-66071 7527 Oak Ridge, TN (United States). doi:10.2172/1254094
- Engel, C., Schattenberg, F., Dohnt, K., Schröder, U., Müller, S., and Krull, R. (2019). Long-term Behavior of Defined Mixed Cultures of *Geobacter Sulfurreducens* and *Shewanella Oneidensis* in Bioelectrochemical Systems. *Front. Bioeng. Biotechnol.* 7, 60. doi:10.3389/fbioe.2019.00060

the manuscript, LB provided analytical support, discussed data and edited the manuscript, MR obtained the funding, discussed experiments and data and edited the manuscript. All authors have given approval to the final version of the manuscript.

FUNDING

Funding for CF fabric research was provided by the German Federal Ministry of Education and Research (BMBF) under grant no. 031B0087A, 031B0087C, and 031B0087D. Further funding for detailed CF fiber research was provided within the IGF research project (IGF grant no. 19047N) of the research association Forschungskuratorium Textil e.V., Reinhardtstraße 14–16, 10117 Berlin, via the AiF within the program for supporting the “Industrial Collective Research” (IGF) from funds of the Federal Ministry of Economic Affairs and Energy (BMWi).

ACKNOWLEDGMENTS

We are very thankful to Michael Brinkmann and Matthias Rave (Güth & Wolf GmbH, Germany), who fabricated and provided full CF leno fabrics (leno-CM1) and discussed their properties. We wish to thank Erika Barcan and Violetta Adiuszyn for the production of mock leno weave fabrics. We also thank Jürgen Klimke (CARBO-TEX GmbH, Germany), who provided plain-CM1 fabrics. Furthermore, we thank Christoph Seitz (ZOLTEK Corporation, Germany), who provided PX35 SB yarns for the production of the leno-SB fabric. We wish to thank Anna Hanisch and Anh Vu Nguyen for their contribution to the experimental work as well as Praveen Iyyappan Valsala for technical support with potentiostats. We also thank Mingze Jiang (MaP Microstructures and Pores GmbH, Germany), who contributed to cross-section image analysis of Cryo-BIB-SEM samples. We acknowledge desizing services by Tim Röding (Institut für Textiltechnik, RWTH Aachen University, Germany).

SUPPLEMENTARY MATERIAL

The Supplementary Material for this article can be found online at: <https://www.frontiersin.org/articles/10.3389/fceng.2022.765682/full#supplementary-material>

- Erben, J., Pinder, Z. A., Lütke, M. S., and Kerzenmacher, S. (2021a). Local Acidification Limits the Current Production and Biofilm Formation of *Shewanella Oneidensis* MR-1 with Electrospun Anodes. *Front. Microbiol.* 12, 1–10. doi:10.3389/fmicb.2021.660474
- Erben, J., Wang, X., and Kerzenmacher, S. (2021b). High Current Production of *Shewanella Oneidensis* with Electrospun Carbon Nanofiber Anodes Is Directly Linked to Biofilm Formation. *ChemElectroChem* 8, 1836–1846. doi:10.1002/celec.202100192
- Farber, P., Gräbel, J., Kroppen, N., Pötschke, L., Roos, D., Rosenbaum, M., et al. (2021). Electricity Generation in a Microbial Fuel Cell with Textile Carbon Fibre Anodes. *Comput. Math. Appl.* 83, 4–23. doi:10.1016/j.camwa.2019.11.019

- Gries, T., Veit, D., and Wulforst, B. (2015). *Textile Technology. An Introduction*. Editor C. Hamilton. 2nd ed. (München, Germany: Carl Hanser Verlag).
- Guo, K., Freguia, S., Dennis, P. G., Chen, X., Donose, B. C., Keller, J., et al. (2013). Effects of Surface Charge and Hydrophobicity on Anodic Biofilm Formation, Community Composition, and Current Generation in Bioelectrochemical Systems. *Environ. Sci. Technol.* 47, 7563–7570. doi:10.1021/es400901u
- Guo, K., PrévotEAU, A., Patil, S. A., and Rabaey, K. (2015). Engineering Electrodes for Microbial Electrocatalysis. *Curr. Opin. Biotechnol.* 33, 149–156. doi:10.1016/j.copbio.2015.02.014
- Guo, K., Soeriyadi, A. H., Patil, S. A., PrévotEAU, A., Freguia, S., Gooding, J. J., et al. (2014). Surfactant Treatment of Carbon Felt Enhances Anodic Microbial Electrocatalysis in Bioelectrochemical Systems. *Electrochem. Commun.* 39, 1–4. doi:10.1016/j.elecom.2013.12.001
- Jourdin, L., and Burdyny, T. (2021). Microbial Electrosynthesis: Where Do We Go from Here? *Trends Biotechnol.* 39, 359–369. doi:10.1016/j.tibtech.2020.10.014
- Kim, J. R., Min, B., and Logan, B. E. (2005). Evaluation of Procedures to Acclimate a Microbial Fuel Cell for Electricity Production. *Appl. Microbiol. Biotechnol.* 68, 23–30. doi:10.1007/s00253-004-1845-6
- Kipf, E., Koch, J., Geiger, B., Erben, J., Richter, K., Gescher, J., et al. (2013). Systematic Screening of Carbon-Based Anode Materials for Microbial Fuel Cells with *Shewanella Oneidensis* MR-1. *Bioresour. Technol.* 146, 386–392. doi:10.1016/j.biortech.2013.07.076
- Kipf, E., Zengerle, R., Gescher, J., and Kerzenmacher, S. (2014). How Does the Choice of Anode Material Influence Electrical Performance? A Comparison of Two Microbial Fuel Cell Model Organisms. *ChemElectroChem* 1, 1849–1853. doi:10.1002/celc.201402036
- Kowtsch, C., Hoffmann, G., and Kleicke, R. (2011). “[German] Gewebte Halbzeuge und Webtechniken,” in *Textile Werkstoffe für den Leichtbau*. Editor C. Cherif (Berlin Heidelberg: Springer), 171–223. doi:10.1007/978-3-642-17992-1
- Liu, J., Liu, J., He, W., Qu, Y., Ren, N., and Feng, Y. (2014). Enhanced Electricity Generation for Microbial Fuel Cell by Using Electrochemical Oxidation to Modify Carbon Cloth Anode. *J. Power Sources* 265, 391–396. doi:10.1016/j.jpowsour.2014.04.005
- Lovley, D. R. (2006). Bug Juice: Harvesting Electricity with Microorganisms. *Nat. Rev. Microbiol.* 4, 497–508. doi:10.1038/nrmicro1442
- Manis, F., Stegshuster, G., Wölling, J., and Schlichter, S. (2021). Influences on Textile and Mechanical Properties of Recycled Carbon Fiber Nonwovens Produced by Carding. *J. Compos. Sci.* 5, 209. doi:10.3390/jcs5080209
- Morgan, P. (2005). *Carbon Fibers and Their Composites*. Boca Raton, FL, USA: CRC Press, Taylor and Francis Group.
- Moß, C., Patil, S. A., and Schröder, U. (2019). Scratching the Surface-How Decisive Are Microscopic Surface Structures on Growth and Performance of Electrochemically Active Bacteria? *Front. Energy Res.* 7, 18. doi:10.3389/fenrg.2019.00018
- Nevin, K. P., Richter, H., Covalla, S. F., Johnson, J. P., Woodard, T. L., Orloff, A. L., et al. (2008). Power Output and Coulombic Efficiencies from Biofilms of *Geobacter Sulfurreducens* Comparable to Mixed Community Microbial Fuel Cells. *Environ. Microbiol.* 10, 2505–2514. doi:10.1111/j.1462-2920.2008.01675.x
- Pötschke, L., Huber, P., Schriever, S., Rizzotto, V., Gries, T., Blank, L. M., et al. (2019). Rational Selection of Carbon Fiber Properties for High-Performance Textile Electrodes in Bioelectrochemical Systems. *Front. Energy Res.* 7, 100. doi:10.3389/fenrg.2019.00100
- Pötschke, L., Stegshuster, G., Molls, C., Klopp, K., Farber, P., Bastian, D., et al. (2018). [German] *Textile Kohlenstoffelektroden für mikrobielle Brennstoffzellen (TexKoMBZ): Schlussbericht zur Machbarkeitsphase*. Aachen: RWTH Aachen University. doi:10.2314/KXP:1667014595
- Rosa, L. F. M., Hunger, S., Zschernitz, T., Strehlitz, B., and Harnisch, F. (2019). Integrating Electrochemistry into Bioreactors: Effect of the Upgrade Kit on Mass Transfer, Mixing Time and Sterilizability. *Front. Energy Res.* 7, 98. doi:10.3389/fenrg.2019.00098
- Santoro, C., Arbizzani, C., Erable, B., and Ieropoulos, I. (2017). Microbial Fuel Cells: From Fundamentals to Applications. A Review. *J. Power Sources* 356, 225–244. doi:10.1016/j.jpowsour.2017.03.109
- Schmatz, J., Klaver, J., Jiang, M., and Urai, J. L. (2017). Nanoscale Morphology of Brine/oil/mineral Contacts in Connected Pores of Carbonate Reservoirs: Insights on Wettability from Cryo-BIB-SEM. *Soc. Pet. Eng.* 22, 1374–1384. doi:10.2118/180049-PA
- Schmitz, S., Nies, S., Wierckx, N., Blank, L. M., and Rosenbaum, M. A. (2015). Engineering Mediator-Based Electroactivity in the Obligate Aerobic Bacterium *Pseudomonas Putida* KT2440. *Front. Microbiol.* 6, 1–13. doi:10.3389/fmicb.2015.00284
- Stegshuster, G., and Schlichter, S. (2018). Perspectives of Web Based Composites from RCF Material. *IOP Conf. Ser. Mat. Sci. Eng.* 406, 012022. doi:10.1088/1757-899X/406/1/012022
- Torres, C. I., Kato Marcus, A., and Rittmann, B. E. (2007). Kinetics of Consumption of Fermentation Products by Anode-Respiring Bacteria. *Appl. Microbiol. Biotechnol.* 77, 689–697. doi:10.1007/s00253-007-1198-z
- Torres, C. I., Marcus, A. K., Lee, H.-S., Parameswaran, P., Krajmalnik-Brown, R., Rittmann, B. E., et al. (2010). A Kinetic Perspective on Extracellular Electron Transfer by Anode-Respiring Bacteria. *FEMS Microbiol. Rev.* 34, 3–17. doi:10.1111/j.1574-6976.2009.00191.x
- You, S., Zhao, Q., Zhang, J., Jiang, J., Wan, C., Du, M., et al. (2007). A Graphite-Granule Membrane-Less Tubular Air-Cathode Microbial Fuel Cell for Power Generation under Continuously Operational Conditions. *J. Power Sources* 173, 172–177. doi:10.1016/j.jpowsour.2007.07.063
- Zhuang, L., Zheng, Y., Zhou, S., Yuan, Y., Yuan, H., and Chen, Y. (2012). Scalable Microbial Fuel Cell (MFC) Stack for Continuous Real Wastewater Treatment. *Bioresour. Technol.* 106, 82–88. doi:10.1016/j.biortech.2011.11.019

Conflict of Interest: GS was employed by the Institut für Textiltechnik Augsburg GmbH. JS was employed by Microstructures and Pores GmbH (MaP).

The remaining authors declare that the research was conducted in the absence of any commercial or financial relationships that could be construed as a potential conflict of interest.

Publisher’s Note: All claims expressed in this article are solely those of the authors and do not necessarily represent those of their affiliated organizations, or those of the publisher, the editors and the reviewers. Any product that may be evaluated in this article, or claim that may be made by its manufacturer, is not guaranteed or endorsed by the publisher.

Copyright © 2022 Pötschke, Huber, Stegshuster, Schriever, Kroppen, Schmatz, Gries, Blank, Farber and Rosenbaum. This is an open-access article distributed under the terms of the Creative Commons Attribution License (CC BY). The use, distribution or reproduction in other forums is permitted, provided the original author(s) and the copyright owner(s) are credited and that the original publication in this journal is cited, in accordance with accepted academic practice. No use, distribution or reproduction is permitted which does not comply with these terms.